

involved in cell penetration and motility, which are *in vitro* parameters for metastasis (23). Likewise, reduction or loss of *ME491* expression is associated with increased metastatic ability of human malignant melanoma (22). Further studies are needed to clarify the functional roles of these genes in tumor metastasis.

REFERENCES AND NOTES

- S. A. Rosenberg, *Surgical Treatment of Metastatic Cancer* (Lippincott, Philadelphia, 1987); L. A. Liotta, P. S. Steeg, W. G. Stetler-Stevenson, *Cell* **64**, 327 (1991); G. L. Nicolson, *Bioessays* **13**, 337 (1991); P. S. Steeg, *Curr. Opin. Oncol.* **4**, 134 (1992).
- I. A. Ramshaw, S. Carlsen, H. C. Wang, P. Badenoch-Jones, *Int. J. Cancer* **32**, 471 (1983); E. Sidebottom and S. R. Clark, *Br. J. Cancer* **47**, 399 (1983).
- T. Ichikawa, Y. Ichikawa, J. T. Isaacs, *Cancer Res.* **51**, 3788 (1991).
- T. Ichikawa *et al.*, *ibid.* **52**, 3486 (1992).
- D. L. Nelson *et al.*, *Proc. Natl. Acad. Sci. U.S.A.* **86**, 6686 (1989).
- AT6.1 is a highly metastatic Dunning rat prostate cancer cell line. Microcell hybrid AT6.1-11-1 contains a fragment of human chromosome 11 from the centromere to region p13 and was suppressed for metastatic ability. Microcell hybrids AT6.1-11-2 and AT6.1-11-3 contain smaller fragments of human chromosome 11 from the centromere to region p11.2 and were not suppressed for metastatic ability (4).
- Clones were obtained as follows: Polyadenylated RNA was isolated from exponentially growing AT6.1-11-1 cells with the FastTrack mRNA isolation kit (Invitrogen, San Diego, CA). A cDNA library for AT6.1-11-1 was constructed in a pSPORT 1 vector with the SuperScript Plasmid System (Gibco BRL). Human Alu sequence primer Alu 559 (5) was used to amplify genomic DNA from the suppressed hybrid AT6.1-11-1 and from the nonsuppressed clone AT6.1-11-2 by PCR. The multiple Alu-PCR fragments from AT6.1-11-1 were cloned into a T-tailed vector, pCR1000 (Invitrogen). Individual clones corresponding to each fragment of these Alu-PCR products were isolated after comparison of the sizes of the Alu-PCR products to molecular weight markers in agarose gel stained with ethidium bromide. Eleven fragments unique to AT6.1-11-1 were labeled by random priming (Gibco BRL) and were used to screen 5×10^4 recombinants of the cDNA library under stringent wash conditions [65°C in 0.1× standard saline citrate (SSC) and 0.1% SDS for 30 min]. Five independent clones were obtained, and their inserts were sequenced with the Sequenase kit (U.S. Biochemical, Cleveland, OH). DNA sequences were analyzed with the GCG package, version 7.3 (Genetics Computer Group, Inc., Madison, WI).
- Southern and Northern blots were hybridized to the *KAI1* probe at 68°C in QuikHyb hybridization solution (Stratagene), washed at 68°C for 30 min in 0.1× SSC and 0.1% SDS, and autoradiographed. The *KAI1* probe was generated by PCR with primers 5'-AGTCTCCCTGCTGCTGTGTG-3' and 5'-TCAGT-CAGGGTGGGCAAGAGG-3' and with *KAI1* cDNA as template. Human and rat β -actin probes were generated by PCR with primers and templates obtained from Clontech (Palo Alto, CA).
- J.-T. Dong and J. C. Barrett, unpublished results.
- T. Imai *et al.*, *J. Immunol.* **149**, 2879 (1992); K. Fukudome *et al.*, *J. Virol.* **66**, 1394 (1992).
- H. W. Gaugitsch, E. Hofer, N. E. Huber, E. Schnabl, T. Baumruker, *Eur. J. Immunol.* **21**, 377 (1991).
- M. L. Gil *et al.*, *J. Immunol.* **148**, 2826 (1992).
- D. Eliyahu, D. Michalovitz, S. Eliyahu, K. Pinhasi, M. Oren, *Proc. Natl. Acad. Sci. U.S.A.* **86**, 8763 (1989).
- KAI1* cDNA was cloned into plasmid pCMVneo, in which transcription is driven by the constitutive human cytomegalovirus promoter (13). The resultant plasmid pCMV-*KAI1* was transfected into AT6.1 cells by the calcium phosphate precipitate method. Individual transfectants were isolated in selection medium. Exponentially growing vector or *KAI1* transfectants were collected by scraping, and cell clumps were broken up by gentle pipetting. The cell suspension was placed in a tube and allowed to stand at room temperature for 30 min. Cells from the supernatant suspension were collected, washed, and resuspended in cold phosphate-buffered saline at 10^6 cells/ml. Male Ncr *nu/nu* nude mice 4 to 5 weeks old were injected with 10^5 cells (0.1 ml) subcutaneously at right and left midlateral sites, about one-fourth of the distance from the base of the skull to the base of the tail. About 6 weeks after injection, the tumors were weighed and the lungs were inflated with Bouin's solution. Tumor foci on the surfaces of lungs were scored under a dissecting microscope.
- M. E. Kaighn, K. Shankar Narayan, Y. Ohnuki, J. F. Lechner, L. W. Jones, *Invest. Urol.* **17**, 16 (1979); J. S. Horoszewicz *et al.*, in *Models for Prostate Cancer*, G. P. Murphy, Ed. (Liss, New York, 1980), pp. 115-132; D. D. Mickey *et al.*, in *ibid.*, pp. 67-84; T. Izumi, T. Yazaki, S. Kanoh, I. Kondo, K. Koiso, *J. Urol.* **137**, 1304 (1987).
- Parental AT6.1 cells, cell hybrid clone AT6.1-11-1, and *KAI1* transfectant were inoculated into the legs of SCID mice (5×10^5 cells per mouse). When tumors reached 3 to 5 cm³, the legs with tumors were surgically removed and the mice were followed until 50 to 60 days after inoculation. Lung metastases for each mouse were analyzed as described (14). For AT6.1, all nine mice had lung metastases, with an average of 83 per mouse. For AT6.1-11-1, four of nine mice had lung metastases, with an average of 6 per mouse. For AT6.1KAI-1, two of seven mice had lung metastases, with an average of 2 per mouse.
- C. W. Rinker-Schaeffer *et al.*, *Cancer Res.* **54**, 6249 (1994).
- J.-T. Dong and J. T. Isaacs, unpublished results.
- Boyden chamber invasion assays were performed as described [J. Vukanovic *et al.*, *Cancer Res.* **53**, 1833 (1993)] with the use of matrigel-coated filters (Collaborative Biomedical Products, Bedford, MA) and 5% fetal bovine serum as chemoattractant in the lower well. After 12 hours of incubation, 19 ± 3 parental AT6.1 cells per 400× field invaded through the matrigel filters, versus 10 ± 2 for the metastasis-suppressed AT6.1-11-1 hybrid cells and 18 ± 2 for the nonsuppressed AT6.1-11-2 hybrid cells.
- J.-T. Dong and J. C. Barrett, unpublished results.
- V. Horejsi and C. Vleck, *FEBS Lett.* **288**, 1 (1991).
- H. Hotta *et al.*, *Cancer Res.* **48**, 2955 (1988); M. Kondoh, M. Ueda, M. Ichihashi, Y. Mishima, E. J. Favalaro, *Melanoma Res.* **3**, 241 (1993); M. J. Metzelaar *et al.*, *J. Biol. Chem.* **266**, 3239 (1991).
- M. Miyake, M. Koyama, M. Seno, S. Ikeyama, *J. Exp. Med.* **174**, 1347 (1991); C. Boucheix *et al.*, *J. Biol. Chem.* **266**, 117 (1991).
- R. Oren *et al.*, *Mol. Cell. Biol.* **10**, 4007 (1990); S. Levy *et al.*, *J. Biol. Chem.* **266**, 14597 (1991).
- B. J. Classon, A. F. Williams, A. C. Willis, B. Seed, I. Stakenkovic, *J. Exp. Med.* **169**, 1497 (1989).
- M. Amiot, *J. Immunol.* **145**, 4322 (1990).
- N. Sharon and H. Lis, *Science* **246**, 227 (1989); K. Drickamer and J. Carver, *Curr. Opin. Struct. Biol.* **2**, 653 (1992).
- S.-I. Hakomori, *Adv. Cancer Res.* **52**, 257 (1989); J. W. Dennis, S. Laferté, C. Waghorne, M. L. Breitman, R. S. Kerbel, *Science* **236**, 582 (1987); M. Ishikawa *et al.*, *Cancer Res.* **48**, 665 (1988).
- Abbreviations for the amino acid residues are as follows: A, Ala; C, Cys; D, Asp; E, Glu; F, Phe; G, Gly; H, His; I, Ile; K, Lys; L, Leu; M, Met; N, Asn; P, Pro; Q, Gln; R, Arg; S, Ser; T, Thr; V, Val; W, Trp; and Y, Tyr.
- We thank R. W. Wiseman, R. D. Owen, L. A. Annab, and P. A. Futreal for advice and B. Vogelstein for plasmid pCMVneo. Supported in part by NIH grant CA 58236 and by the NIH Office of Minority Health Research.

6 December 1994; accepted 17 February 1995

Long-Range Motional Restrictions in a Multidomain Zinc-Finger Protein from Anisotropic Tumbling

Rafael Brüsweiler,* Xiubei Liao,† Peter E. Wright‡

Structural characterization of biomolecules in solution by nuclear magnetic resonance (NMR) spectroscopy is based primarily on the use of interproton distances derived from homonuclear cross-relaxation experiments. Information about short time-scale dynamics, on the other hand, is obtained from relaxation rates of heteronuclear spin pairs such as ¹⁵N-¹H. By combining the two types of data and utilizing the dependence of heteronuclear NMR relaxation rates on anisotropic diffusional rotational tumbling, it is possible to obtain structural information about long-range motional correlations between protein domains. This approach was applied to characterize the relative orientations and mobilities of the first three zinc-finger domains of the *Xenopus* transcription factor TFIIIA in aqueous solution. The data indicate that the motions of the individual zinc-finger domains are highly correlated on time scales shorter than 10 nanoseconds and that the average conformation of the three-finger polypeptide is elongated.

Proteins of modular architecture, assembled from independently folded domains, are common in eukaryotes and play an important role in such fundamental events as transcriptional regulation, signal transduc-

tion, and blood coagulation. Characterization of the interdomain spatial interactions and motions is essential for understanding the function and biological activity of modular proteins. NMR spin relaxation measurements offer the potential for characterizing the flexibility and overall solution structure of multidomain proteins, even when most interdomain proton-proton distances exceed the 5 Å limit for observation of the nuclear Overhauser effect (NOE).

Orientational correlations between protein domains can induce anisotropic overall

Department of Molecular Biology, Scripps Research Institute, La Jolla, CA 92037, USA.

*Present address: Laboratorium für Physikalische Chemie, Eidgenössische Technische Hochschule Zentrum, 8092 Zürich, Switzerland.

†Present address: Department of Biochemistry, University of Illinois, Chicago, IL 60612, USA.

‡To whom correspondence should be addressed.

rotational tumbling, which affects NMR spin relaxation (1). This effect can be exploited to characterize average interdomain orientations in multidomain proteins on the basis of the corresponding rotational diffu-

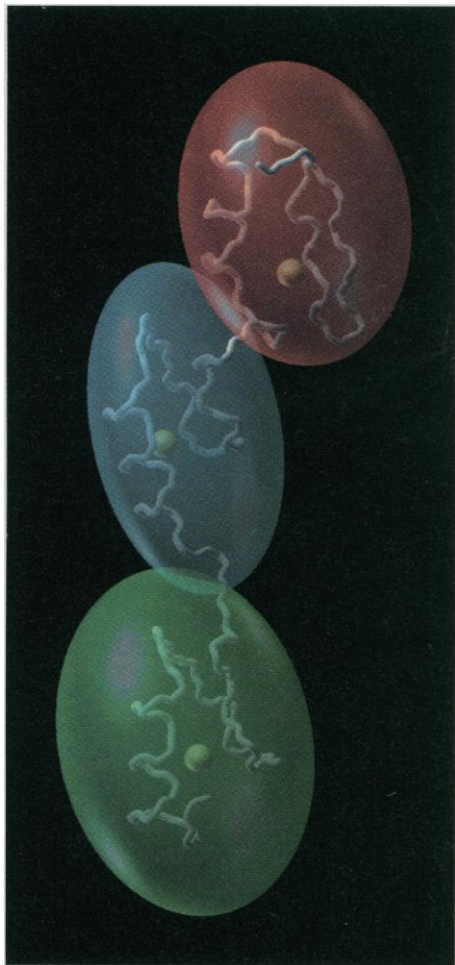


Fig. 1. Model for the averaged alignment of the three zinc-finger domains of ZF1-3 (first three domains of transcription factor TFIIIA) obtained from anisotropic rotational tumbling effects manifested in heteronuclear NMR relaxation data. The molecule is, on average, highly elongated. The ellipsoids superimposed on the three zinc-finger domains represent the rotational diffusion tensors from Table 1. The three domains are oriented such that their diffusion tensors are aligned with respect to each other. The peptide backbone and the position of the zinc atom in each finger are shown in white. The ellipsoid of the NH₂-terminal domain (ZF1) is red, that of the middle domain (ZF2) is blue, and that of the COOH-terminal domain (ZF3) is green. The lengths of the principal axes of each ellipsoid are proportional to the rotational diffusion coefficients D_{xx} , D_{yy} , and D_{zz} for the corresponding zinc-finger domain. The relative sizes and shapes of the ellipsoids reflect the differential mobilities of the zinc-finger domains. The blue ellipsoid is the smallest and most anisotropic and reflects the slow and restricted rotational tumbling of ZF2 relative to the other two zinc fingers. The largest ellipsoid is that of ZF3 (its size indicates that this domain has the greatest motional freedom).

sion tensors derived from ¹⁵N relaxation data. The spin relaxation rates depend on the average orientations of the ¹⁵N-¹H internuclear vectors and on their fluctuations relative to the diffusion tensor. In this way dynamic long-range correlations can be assessed, thereby extending structural information from homonuclear cross-relaxation rates and scalar J -coupling constants. This approach can generally be used to characterize long-range order in modular proteins, provided that they exhibit significant tumbling anisotropy. We illustrate the method with a polypeptide, termed ZF1-3 (2), which contains 92 amino acids and consists of the first three Cys₂-His₂ zinc-finger domains of the *Xenopus* transcription factor TFIIIA (3). This protein binds with high affinity and specificity to the C-block element of the internal control region of the 5S RNA gene (2, 4, 5).

Heteronuclear protein backbone ¹⁵N NMR relaxation parameters, consisting of longitudinal relaxation rates T_1 , transverse relaxation rates T_2 , and the ¹⁵N {¹H} NOE (η) were measured (6, 7) in standard multidimensional inverse-detected NMR experiments (8, 9). Generally, anisotropic rotational diffusion of a rigid molecule (asymmetric top) is characterized by its diffusion tensor \mathbf{D} of rank 2 (10), which can be represented by a symmetric 3×3 matrix and is defined by six parameters, such as the lengths of the three principal axes D_{xx} , D_{yy} , and D_{zz} and the Euler angles α , β , and γ , which determine the orientation of the tensor (diffusion frame) with respect to a molecule-fixed reference frame. A diffusion tensor can be conveniently visualized by a three-dimensional ellipsoid (see Fig. 1), which represents the rate of rotational tumbling about arbitrary axes.

For each ¹⁵N-¹H pair, overall tumbling and fast internal dynamics are separable according to the model-free formalism (11), where the power spectral density function at the ¹⁵N site is parametrized as

$$J_i(\omega) = S_i^2 \frac{2\tau_{c,i}}{1 + \omega^2\tau_{c,i}^2} + (1 - S_i^2) \frac{2\tau_{\text{eff},i}}{1 + \omega^2\tau_{\text{eff},i}^2}$$

and

$$\tau_{\text{eff},i}^{-1} = \tau_{c,i}^{-1} + \tau_{\text{int},i}^{-1} \quad (1)$$

where i specifies the ¹⁵N-¹H pair, $\tau_{c,i}$ is its overall tumbling correlation time, S_i^2 is the order parameter that describes the spatial restriction of intramolecular motion of the internuclear ¹⁵N-¹H vector, and $\tau_{\text{int},i}$ is the associated effective internal correlation time. The three parameters $\tau_{c,i}$, S_i^2 , and $\tau_{\text{int},i}$ can be determined from experimental values of $T_{1,i}$, $T_{2,i}$, and η_i by a least squares fit (11). In the case of anisotropic rotational diffusion, the $\tau_{c,i}$ values depend on the directions of the ¹⁵N-¹H vectors relative to the diffusion tensor, and we use this geo-

metric information in the following to describe preferential orientations and mobilities of protein domains. In contrast, for a spherical top, which is most commonly assumed for the interpretation of NMR relaxation data, $\tau_{c,i}$ is direction-independent and thus contains no information on structure.

It can be shown that, for small anisotropies of the diffusion tensor, the $\tau_{c,i}$ values follow a representation quadric

$$(6\tau_{c,i})^{-1} = \mathbf{e}_i^T \mathbf{D} \mathbf{e}_i \quad (2)$$

where \mathbf{e}_i is the normalized interatomic vector of ¹⁵N-¹H pair i . The eigenvectors of \mathbf{D} define the principal axes of the diffusion tensor, and the three eigenvalues D_1 , D_2 , and D_3 are related to the rotational diffusion constants D_{xx} , D_{yy} , and D_{zz} by

$$\begin{aligned} D_{xx} &= -D_1 + D_2 + D_3 \\ D_{yy} &= D_1 - D_2 + D_3 \\ D_{zz} &= D_1 + D_2 - D_3 \end{aligned} \quad (3)$$

For a set of N ¹⁵N-¹H vectors $\{\mathbf{e}_i\}$ with correlation times $\{\tau_{c,i}\}$, the diffusion tensor \mathbf{D} can be determined by a linear least squares fit provided that the set $\{\mathbf{e}_i\}$ represents a sufficiently wide distribution of directions. The presence of secondary structure introduces orientational correlations between the ¹⁵N-¹H vectors and thus reduces the effective number of independent data points. The degree of overdetermination of the linear least squares optimization problem of Eq. 2 can be assessed in the usual way by means of the condition number obtained from a singular value decomposition, and the quality of the model can be characterized by the goodness of fit based on the minimum χ^2 (12). Equation 2 describes the general case of an asymmetric top, which is the model of choice in the absence of molecular symmetries.

Diffusion tensors have been determined individually for each of the three zinc-finger domains in ZF1-3. For this purpose, a set of 29 structures of ZF1-3 has been generated from experimental NOE spectroscopy cross-relaxation data complemented by NH-H _{α} coupling constants (13). Each of the three zinc-finger domains has a well-defined structure and displays the canonical zinc-finger fold (14), a small globular motif formed from a β hairpin and an α helix that ligates a zinc ion. Only very few interdomain NOEs could be detected (13), all of them between the NH₂-terminal zinc finger (ZF1) and the middle finger (ZF2). These interdomain NOEs involve residues Asp¹⁰ and His²⁸ of ZF1 and Phe⁴⁵ and Thr⁴⁶ of ZF2 and are indicative of interactions between the domains. However, with so few interdomain NOEs, the relative orientations of the domains are ill-defined (13), as reported for the first two zinc-finger domains of SW15 (15). In contrast, many

NOEs were observed between the finger domains from the human immunodeficiency virus (HIV) enhancer binding protein, leading to a reasonably well-defined interdomain orientation (16).

We extracted an averaged diffusion tensor separately for each zinc-finger domain by first aligning the backbones for each finger, and then determining the individual diffusion tensors based on Eq. 2. Because the extracted diffusion tensors are sensitive to local structure (e_i orientations), only n_α tensors yielding goodness-of-fit values above 0.1 and condition numbers less than 5 have been included in the averaging

$$\mathbf{D}_\alpha = n_\alpha^{-1} \sum_{n=1}^{n_\alpha} \mathbf{D}_\alpha^{(n)} \quad (4)$$

where α indicates the domains (ZF1, ZF2, or ZF3). Because the backbone ^{15}N - ^1H vector orientations for the two linkers (Thr²⁹-Pro³³ and Thr⁵⁹-Asn⁶³) are ill-defined in the NMR structures, they were not included in the diffusion tensor calculations. The resulting diffusion tensors (summarized in Table 1) show substantial amounts of anisotropy and asymmetry, with the largest effects belonging to ZF2. Protein aggregation does not appear to contribute to the slow, anisotropic tumbling of ZF1-3 (17).

Table 2 gives the results for two simpler models based on isotropic overall tumbling. Model I assumes that the three domains tumble as a single spherical top, and model II treats each domain as an independent spherical top with an individual correlation time. Both models take fast intradomain dynamics into account in the model-free way (11). Models I and II yield average tumbling correlation times of ~ 9 ns, which is consistent with the anisotropic tumbling model (Table 1) and much larger than the 1.8 ns obtained for a single zinc finger (18). These correlation times imply that the tumbling motions of the three fingers are highly

Table 1. Reorientational diffusion tensors of ZF1-3. For each domain, the diffusion constants D_{xx} , D_{yy} , and D_{zz} of the anisotropic rotational diffusion tensor \mathbf{D} calculated as linear averages over the best fitting diffusion tensors, are expressed in terms of correlation times. The goodness-of-fit values give a measure of the agreement between experimental and calculated $\tau_{c,i}$ values for the three domains. Residues that experience "true" exchange contributions (Ala⁹, Thr⁵², Asp⁷², and Ala⁷⁹) as defined by Barbato *et al.* (19), were excluded from the fit.

Do-main	Diffusion constants (ns)			Goodness of fit
	$(6D_{xx})^{-1}$	$(6D_{yy})^{-1}$	$(6D_{zz})^{-1}$	
ZF1	10.9	8.5	7.2	0.2
ZF2	15.1	9.4	6.6	0.3
ZF3	10.1	7.6	6.3	0.1

correlated on the sub-10-ns time scale. The low goodness-of-fit values, however, indicate that isotropic tumbling models cannot satisfactorily explain all aspects of the relaxation data.

The overall tumbling of ZF1-3 is both anisotropic and much slower than expected for a single zinc finger (18), suggesting the presence of interactions among the three domains and motional restrictions imposed by the linkers. The average solution conformation of the three-zinc-finger protein is significantly elongated. Interconversion of interdomain arrangements on slow time scales ($50 \text{ ns} < \tau < 1 \text{ ms}$) causes diffusion tensor fluctuations $\mathbf{D}(t)$, which give rise to an averaged tensor

$$\bar{\mathbf{D}} = \sum_j p_j \mathbf{D}^{(j)} \quad (5)$$

where the sum includes all arrangements j with populations p_j . The fitting procedure based on Eq. 2 yields in this case an averaged tensor $\bar{\mathbf{D}}$ but does not allow characterization of the $\mathbf{D}^{(j)}$ tensors belonging to the various populated substates. Such rearrangements may or may not affect the average tumbling correlation time and tend to decrease the effective rotational anisotropy.

Differences in the size of two diffusion tensors belonging to the domains α and β (for example, \mathbf{D}_{ZF1} and \mathbf{D}_{ZF2}) can be expressed by the parameter $\kappa_{\alpha\beta}$

$$\kappa_{\alpha\beta} = \frac{\text{Tr}(\mathbf{D}_\alpha)}{\text{Tr}(\mathbf{D}_\beta)} \quad (6)$$

(where $\alpha, \beta = \text{ZF1, ZF2, ZF3}$, and Tr indicates the matrix trace) which is a measure of differential rotational diffusion between the two domains. Deviations of the κ parameters from unity indicate that the three domains do not tumble as a fully rigid entity and that rigid-body motion on time scales of the order of the tumbling rate is present. Consequently, the COOH-terminal ZF3 domain is most mobile ($\kappa_{\text{ZF3,ZF2}} = 1.20$), followed by ZF1 ($\kappa_{\text{ZF1,ZF2}} = 1.08$). The central ZF2 domain is least mobile, because it is restricted in its motional freedom from both ends by ZF1 and ZF3. For the same reason, diffusional anisotropy and asymmetry are largest for ZF2 (Table 1). Intradomain dynamics, expressed by the model-free

Table 2. Isotropic tumbling models. Model I assumes that all three domains (ZF1, ZF2, and ZF3) tumble isotropically as a single sphere, and model II assumes that each domain tumbles individually as a sphere.

Model	$(6D_{\text{ZF1}})^{-1}$ (ns)	$(6D_{\text{ZF2}})^{-1}$ (ns)	$(6D_{\text{ZF3}})^{-1}$ (ns)	Goodness of fit
I		8.6		10^{-36}
II	8.7	9.9	7.9	6×10^{-8}

parameters S^2 and τ_{int} , is rather constrained with average $S^2 = 0.82$ and time scales shorter than 100 ps. The two linker regions are also restricted in their mobility on sub-nanosecond time scales, with average $S^2 = 0.7$. In this regard, the linkers in ZF1-3 behave differently from the linker connecting the two EF hand-type domains in calmodulin, where it was concluded from NMR relaxation data that the linker is flexible and that the two domains exhibit essentially isotropic, uncorrelated motions in the sub-10-ns time window (19).

The anisotropic tumbling behavior observed for ZF1-3 arises from correlated diffusional motions of the individual zinc-finger domains on a time scale of about 10 ns. This means that the principal axes of the diffusion tensors of the three zinc-finger domains should display approximate alignment because they reflect the overall shape of the whole molecule. It is therefore possible to determine the average solution conformation of the protein by orienting the individual zinc-finger domains such that their principal diffusion axes are aligned in parallel. Although the alignment of the individual diffusion tensors cannot be specified uniquely (20), the two linkers impose substantial steric restrictions on the possible arrangements of the three zinc-finger domains.

One possible average interdomain arrangement is depicted in Fig. 1, which shows the three zinc-finger domains superimposed on their respective diffusion tensors represented as ellipsoids. Although restricted rigid-body motions of the individual zinc-finger domains do occur, as reflected in the different sizes and shapes of the ellipsoids, the overall structure of the protein in solution is highly elongated on average.

The motional restrictions of the individual zinc-finger domains could be of biological significance in that they lower the entropic costs of DNA binding and might also affect the kinetics and selectivity early in the docking event. Indeed, Radhakrishnan *et al.* have recently found (21) that a single site mutation in the first linker of ZF1-3 that results in decreased DNA binding affinity (22) also leads to enhanced flexibility in the linker between the first two finger domains in the free zinc-finger protein.

REFERENCES AND NOTES

- D. E. Woessner, *J. Chem. Phys.* **37**, 647 (1962); W. T. Huntress, *ibid.* **48**, 3524 (1967).
- X. Liao, K. R. Clemens, L. Tennant, P. E. Wright, J. M. Gottesfeld, *J. Mol. Biol.* **223**, 857 (1992).
- J. Miller, A. D. McLachlan, A. Klug, *EMBO J.* **4**, 1609 (1985).
- K. R. Clemens, X. Liao, V. Wolf, P. E. Wright, J. M. Gottesfeld, *Proc. Natl. Acad. Sci. U.S.A.* **89**, 10822 (1992).
- J. H. Christensen, P. K. Hansen, O. Lillelund, H. C. Thøgersen, *FEBS Lett.* **281**, 181 (1991).
- Uniformly ^{15}N -labeled ZF1-3 was obtained by over-

Borders of Multiple Visual Areas in Humans Revealed by Functional Magnetic Resonance Imaging

M. I. Sereno,* A. M. Dale, J. B. Reppas, K. K. Kwong, J. W. Belliveau, T. J. Brady, B. R. Rosen, R. B. H. Tootell

The borders of human visual areas V1, V2, VP, V3, and V4 were precisely and noninvasively determined. Functional magnetic resonance images were recorded during phase-encoded retinal stimulation. This volume data set was then sampled with a cortical surface reconstruction, making it possible to calculate the local visual field sign (mirror image versus non-mirror image representation). This method automatically and objectively outlines area borders because adjacent areas often have the opposite field sign. Cortical magnification factor curves for striate and extrastriate cortical areas were determined, which showed that human visual areas have a greater emphasis on the center-of-gaze than their counterparts in monkeys. Retinotopically organized visual areas in humans extend anteriorly to overlap several areas previously shown to be activated by written words.

Over half of the neocortex in nonhuman primates is occupied by visual areas. At least 25 visual areas beyond the primary visual cortex (V1) have been identified with a combination of microelectrode mapping, tracer injections, histological stains, and functional studies (1). The analysis of this data has been greatly aided by the use of flattened representations of the cortical surface made from conventional sections with graphical techniques (2) and flattened wire models (3), or more directly from sections of physically flat-mounted cortex (4).

A large portion of the neocortex in humans is likely to be occupied by visual areas too. It has been difficult, however, to outline unambiguously any human cortical area with noninvasive techniques. Previous studies have mapped only a few locations in the visual field or have relied on stimulus features to activate different areas (5), and the tortuous convolutions of the human neocortex have defied previous attempts to see activity across all of its surface area at once.

Many of the cortical visual areas in nonhuman primates are retinotopically organized to some degree (3, 6). These areas are irregularly shaped and somewhat variable in location; consequently, recordings from many locations (400 to 600) in single ani-

mals have been required to define areal borders with confidence (7). Here we demonstrate a technique for generating retinotopic maps of visual cortex in humans with a precision similar to that obtained in the most detailed invasive animal studies. Responses to phase-encoded retinal stimulation (8) were recorded with echo-planar functional magnetic resonance imaging (MRI) (9) and analyzed with a Fourier-based method. The resulting volume data sets were sampled with a cortical surface reconstruction made from high-resolution structural MRI images collected separately for each participant (10). The cortical surface containing the data was then unfolded and analyzed with the visual field sign method to distinguish mirror image from non-mirror image representations (7). By combining these four techniques (multislice functional MRI, stimulus phase-encoding and Fourier analysis, cortical surface reconstruction, and visual field sign calculations), it was possible to reconstruct the retinotopic organization of visual areas V1, V2, VP, V3, and V4 in humans in two dimensions and to accurately trace out the borders between these areas in the living human brain.

To map polar angle (angle from the center-of-gaze), we obtained 128 asymmetric spin echo MRI images (11) of 8 to 16 oblique sections perpendicular to the calcarine sulcus (1024 to 2048 total) in a 512-s session (~8.5 min) while participants ($n = 7$) viewed a slowly rotating (clockwise or counterclockwise), semicircular checkerboard stimulus. Eccentricity (distance from the center-of-gaze) was mapped with a thick ring (dilating or contracting) instead of a semicircle. These four kinds of stimuli elicit periodic excitation at the rotation or dilation-contraction frequency at each point in a cortical retinotopic map (8, 12). The

expression in *Escherichia coli* as described by X. Liao, K. R. Clemens, J. Cavanagh, L. Tennant, and P. E. Wright [*J. Biomol. NMR* **4**, 433 (1994)]. We performed the NMR experiments at 300 K at a ^1H frequency of 500 MHz, using a 0.5 mM solution of ZF1-3 in 30 mM phosphate buffer (pH 6.5) in a mixture of 90% H_2O and 10% D_2O containing 30 mM NaCl, 5 mM deuterated dithiothreitol, and 50 μM ZnCl_2 .

7. Analysis of the data, accounting for both dipolar relaxation of the ^{15}N spin mediated by its directly attached proton and relaxation caused by chemical shielding anisotropy, was based on the classical expressions (8)

$$T_1^{-1} = \sum_j a_j J(\omega_j)$$

$$T_2^{-1} = \sum_j b_j J(\omega_j)$$

$$\eta = 1 + \frac{\omega_H}{\omega_N} T_1 \sum_j c_j J(\omega_j)$$

with constant coefficients a_j , b_j , and c_j . The power spectral density $J(\omega)$ reflects molecular dynamics processes (intramolecular dynamics as well as overall rotational tumbling) and is sampled at frequencies ω_j , which are combinations of the ^{15}N and ^1H Larmor frequencies ω_N and ω_H .

8. L. E. Kay, D. A. Torchia, A. Bax, *Biochemistry* **28**, 8972 (1989).
9. M. J. Stone *et al.*, *ibid.* **31**, 4394 (1992).
10. P. Debye, *Polar Molecules* (Dover, New York, 1929), chap. 5; F. Perrin, *J. Phys. Radium* **5**, 497 (1934); *ibid.* **7**, 1 (1936); L. D. Favro, *Phys. Rev.* **107**, 7 (1960).
11. G. Lipari and A. Szabo, *J. Am. Chem. Soc.* **104**, 4546 (1982).
12. W. H. Press, B. P. Flannery, S. A. Teukolsky, W. T. Vetterling, *Numerical Recipes in C: The Art of Scientific Computing* (Cambridge Univ. Press, Cambridge, 1988).
13. Structures were calculated from 1284 NOE distance constraints and 45 dihedral angle constraints by variable target function distance geometry and restrained molecular dynamics (X. Liao and P. E. Wright, unpublished data).
14. M. S. Lee, G. P. Gippert, K. V. Soman, D. A. Case, P. E. Wright, *Science* **245**, 635 (1989); R. E. Klevit, J. R. Herriott, S. J. Horvath, *Proteins* **7**, 215 (1990).
15. Y. Nakaseko, D. Neuhaus, A. Klug, D. Rhodes, *J. Mol. Biol.* **228**, 619 (1992).
16. J. G. Omichinski *et al.*, *Biochemistry* **31**, 3907 (1992).
17. Contributions from aggregation can be excluded as a result of the excellent agreement found between the effective rotational tumbling correlation time obtained by tryptophan fluorescence depolarization measurements at a ZF1-3 concentration of 50 μM and that derived from NMR relaxation measurements at more than 10-fold higher concentration (X. Liao, R. Brüscheweiler, D. Millar, P. E. Wright, unpublished data).
18. A. G. Palmer, M. Rance, P. E. Wright, *J. Am. Chem. Soc.* **113**, 4371 (1991).
19. G. Barbato, M. Ikura, L. E. Kay, R. W. Pastor, A. Bax, *Biochemistry* **31**, 5269 (1992).
20. It is not possible to specify uniquely the relative orientations of the diffusion tensors as a consequence of the transformation properties of the responsible spin interactions. The relaxation data cannot distinguish between orientations that relate individual domains by an orthorhombic symmetry transformation of the diffusion tensor ellipsoids. This means that a 180° rotation of any of the domains about the x, y, or z axes of their diffusion frames leaves the relaxation parameters unchanged.
21. I. Radhakrishnan, D. Millar, P. E. Wright, unpublished data.
22. K. R. Clemens *et al.*, *J. Mol. Biol.* **244**, 23 (1994).
23. We thank T. Macke for making Fig. 1 (with graphics program AVS) and D. Millar and J. Gottesfeld for helpful discussions. X.L. is a recipient of the Cancer Research Institute-Miriam and Benedict Wolf Fellowship. This work was funded by grant GM 36643 from the National Institutes of Health.

8 November 1994; accepted 21 February 1995

M. I. Sereno, Cognitive Science 0515, University of California, San Diego, La Jolla, CA 92093-0515, USA.

A. M. Dale, Cognitive Science 0515, University of California, San Diego, La Jolla, CA 92093-0515, USA, and Department of Neurophysiology, University of Oslo, 0316 Oslo, Norway.

J. B. Reppas, Harvard-Massachusetts Institute of Technology Division of Health Sciences and Technology, Boston, MA 02115, USA.

K. K. Kwong, J. W. Belliveau, T. J. Brady, B. R. Rosen, R. B. H. Tootell, Massachusetts General Hospital Nuclear Magnetic Resonance Center, 149 13th Street, Charlestown, MA 02129, USA.

*To whom correspondence should be addressed.